

Azimuthal Anamorphic Ray-map for Immersive Renders in Perspective

Jakub Maksymilian Fober
talk@maxfober.space

Abstract

Wide choice of cinematic lenses enables motion-picture creators to adapt image visual-appearance to their creative vision. Such choice does not exist in realm of real-time computer graphics, where only one type of perspective projection is widely used. This work provides perspective imaging model that in an artistically convincing manner resembles anamorphic photography lens variety. It presents anamorphic azimuthal projection map with natural vignetting and realistic chromatic aberration. Mathematical model for this projection has been chosen such that its parameters reflect psycho-physiological aspects of visual perception. That enables use in artistic and professional environments, where specific aspects of the photographed space are to be presented.

CCS Concepts: • Computing methodologies → Perception; Ray tracing; • Human-centered computing; • Applied computing → Media arts;

Keywords: Curvilinear Perspective, Panini, Cylindrical, Fish-eye, Perspective Map

© 2025 Jakub Maksymilian Fober



This work is licensed under Creative Commons BY-NC-ND 3.0 license.
<https://creativecommons.org/licenses/by-nc-nd/3.0/>
For all other uses including commercial, contact the owner/author(s).

1 Introduction

Perspective in computer real-time graphics hasn't changed since the dawn of CGI. It is based on a concept as old as fifteenth century Renaissance, a linear projection [Alberti 1435; Argan and Robb 1946; McArdle 2013]. This situation is similar to beginnings of photography in 1840, where only one type of lens was widely available, a *Rapid Rectilinear* [Kingslake 1989]. Linear perspective even at a time of its advent, 500-years ago, has been criticized for distorting proportions [Da Vinci 1632]. In a phenomenon known today as *Leonardo's paradox* [Dixon 1987]. Computer graphics really skipped artistic achievements of last five centuries in regard to perspective. This includes cylindrical perspective of Pannini [Sharpless et al. 2010], Barker [Wikipedia, contributors 2019] and anamorphic lenses used in cinematography [Giardina 2016; Sasaki 2017a,b]. Situation is critical even

more so, as there is no mathematical model for generating anamorphic projection in an artistically-convincing manner. Some attempts were made at alternative projections for computer graphics, with fixed cylindrical or spherical geometry [Baldwin et al. 2014; Sharpless et al. 2010]. Parametrized perspective model was also proposed as a new standard [Correia and Romão 2007], but wasn't adopted. It included interpolation states in-between rectilinear/equidistant and spherical/cylindrical projection. The cylindrical parametrization of this solution was merely an interpolation factor, where intermediate values did not correspond to any common projection type. Therefore it was not suited for artistic or professional use. Notion of sphere as a projective surface, which incorporates cartographic mapping to produce perspective picture became popularized [German et al. 2007; Peñaranda et al. 2015; Williams 2015]. Also perspective parametrization that transitions according to the content (by the view-tilt angle) has been developed, as a modification to computer game Minecraft [Williams 2017]. But results of these solutions where more a gimmick and have not found practical use. The linear perspective projection is still way-to-go for most digital content. One of the reasons is the GPU fixed-function architecture in regard to rasterization. With an advent of real-time ray-tracing, more exotic projections could become widely adopted.

This paper aims to provide perspective model with mathematical parametrization that gives artistic-style interaction with image-geometry. A parametrization that works similarly to the way film directors choose lenses for each scene by their aesthetics [Giardina 2016; Sasaki 2017a], but with greater degree of control. It also aims to provide psycho-physiological correlation between perspective model parameters and perception of depicted space attributes, like distance, size, proportions, shape or speed. That mapping enables use of presented model in a professional environment, where image geometry is specifically suited to a task [Whittaker 1984].

1.1 Document naming convention

This document uses following naming convention:

- Left-handed coordinate system.
- Vectors presented natively in column.
- Matrix vectors arranged in rows (row-major order)
 $M_{\text{row col}}$.
- Matrix-matrix multiplication by $[\text{column}]' \cdot [\text{row}]_b = M_{ab}$.

- Double bar enclosure “ $\|\vec{A}\|$ ” represent vector direction.
- Single bar enclosure “ $|u|$ ” represent vector length or scalar absolute.
- Vectors with arithmetic sign, or none are calculated component-wise and form another vector.
- Centered dot “ \cdot ” represent vector dot product.
- Cross sign “ \times ” represent vector cross-product.
- Square brackets with comma “[f, c]” denote interval.
- Square brackets with blanks “[$x \ y$]” denote vector, matrix.
- Power of “ -1 ” signifies reciprocal of the value.
- QED symbol “ \square ” marks final result or output.

This naming convention simplifies transformation process of formulations into code.

2 Anamorphic primary-ray map

If we assume that projective visual space is spherical [Fleck 1994; McArdle 2013], one can define perspective picture as an array of rays pointing to the visual sphere surface. This is how the algorithm described below will output a projection-map, aka perspective-map. It is an array of three-dimensional rays, which are assigned to each screen-pixel. Having visual sphere as the image model enables wider angle of view, beyond 180° limit of planar projection. Ray-map can easily be converted to cube UV -map, ST -map and other formats.

Here procedural algorithm for primary-ray map (aka perspective map) uses two input values from the user, distortion parameter for two power axes and *focal-length* or *angle-of-view* (aka FOV). Two distinct power axes define the anamorphic projection type. Each axis is expressed by the azimuthal projection factor k [Bettonvil 2005; Fleck 1994; Krause 2019]. Both power axes share same focal-length f . Evaluation of each power-axis produces spherical angle $\vec{\theta}_x$ and $\vec{\theta}_y$, which are then combined to anamorphic azimuthal-projection angle θ' . Interpolation of θ is done by the anamorphic weight $\vec{\varphi}_x$ and $\vec{\varphi}_y$. Weights are derived from spherical angle φ , of azimuthal projection. To note, calculation of φ is here omitted, using optimization of view-coordinates vector \vec{v} .

$$r = |\vec{v}| = \sqrt{\vec{v}_x^2 + \vec{v}_y^2} \quad (1a)$$

$$\vec{\theta}_x = \begin{cases} \frac{\arctan\left(\frac{r}{f} \vec{k}_x\right)}{k_x}, & \text{if } \vec{k}_x > 0 \\ \frac{r}{f}, & \text{if } \vec{k}_x = 0 \\ \frac{\arcsin\left(\frac{r}{f} \vec{k}_x\right)}{k_x}, & \text{if } \vec{k}_x < 0 \end{cases} \quad (1b)$$

$$\vec{\theta}_y = \begin{cases} \frac{\arctan\left(\frac{r}{f} \vec{k}_y\right)}{k_y}, & \text{if } \vec{k}_y > 0 \\ \frac{r}{f}, & \text{if } \vec{k}_y = 0 \\ \frac{\arcsin\left(\frac{r}{f} \vec{k}_y\right)}{k_y}, & \text{if } \vec{k}_y < 0 \end{cases} \quad (1c)$$

$$\begin{bmatrix} \vec{\varphi}_x \\ \vec{\varphi}_y \end{bmatrix} = \begin{bmatrix} \frac{\vec{v}_x^2}{\vec{v}_x^2 + \vec{v}_y^2} \\ \frac{\vec{v}_y^2}{\vec{v}_x^2 + \vec{v}_y^2} \end{bmatrix} = \begin{bmatrix} \cos^2 \varphi \\ \sin^2 \varphi \end{bmatrix} = \begin{bmatrix} \frac{1}{2} + \frac{\cos(2\varphi)}{2} \\ \frac{1}{2} - \frac{\cos(2\varphi)}{2} \end{bmatrix}, \quad (1d)$$

where $r \in \mathbb{R}_{>0}$ is the view-coordinates radius. Vector $\vec{\theta} \in [0, \pi]^2$ contains incident angles (measured from optical axis) of two azimuthal projections. Vector $\vec{\varphi} \in [0, 1]^2$ is the anamorphic interpolation weight. It is linear $\vec{\varphi}_x + \vec{\varphi}_y = 1$, but has spherical distribution (see Figure 1 on the facing page). Vector $\vec{k} \in [-1, 1]^2$ describes two power axes of anamorphic projection. The algorithm is evaluated per-pixel of position $\vec{v} \in \mathbb{R}^2$ in view-space coordinates, centered at the optical axis and normalized at chosen angle-of-view (horizontal or vertical). The final anamorphic incident angle θ' is obtained by interpolation using $\vec{\varphi}$ weights.

$$\theta' = \begin{bmatrix} \vec{\theta}_x \\ \vec{\theta}_y \end{bmatrix} \cdot \begin{bmatrix} \vec{\varphi}_x \\ \vec{\varphi}_y \end{bmatrix} \quad (2a)$$

$$\begin{bmatrix} \hat{G}_x \\ \hat{G}_y \\ \hat{G}_z \end{bmatrix} = \begin{bmatrix} \frac{\sin \theta'}{r} \begin{bmatrix} \vec{v}_x \\ \vec{v}_y \end{bmatrix} \\ \cos \theta' \end{bmatrix} = \begin{bmatrix} \sin \theta' \begin{bmatrix} \cos \varphi \\ \sin \varphi \end{bmatrix} \\ \cos \theta' \end{bmatrix}, \quad \square \quad (2b)$$

here $\theta' \in (0, \pi]$ is the anamorphic incident angle, measured from the optical axis. This measurement resembles azimuthal projection of the globe (here a visual sphere) [McArdle 2013]. Final incident vector $\hat{G} \in [-1, 1]^3$ (aka primary-ray) is obtained from anamorphic angle θ' . Parameters $r, \vec{v}, \vec{\varphi}$ are in view-space, while $\vec{\theta}, \theta', \varphi, \hat{G}$ are in visual-sphere space. Essentially anamorphic primary-ray map preserves azimuthal angle φ , while scaling only the picture's radius.

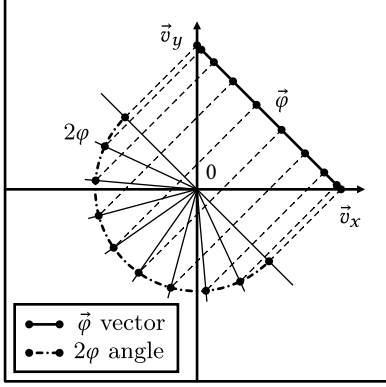
2.1 Focal length and angle-of-view

To give more control over the picture, a mapping between angle-of-view Ω and focal-length f can be established. Here focal-length is derived in a reciprocal from, to optimize usage in Equation (1).

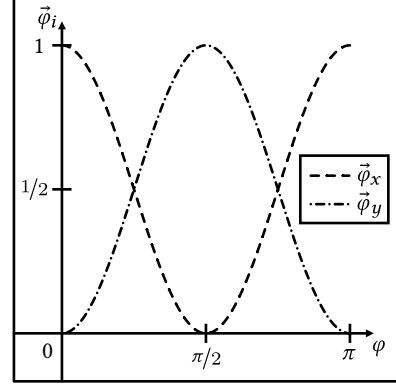
$$f^{-1}(\Omega_h) = \begin{cases} \frac{\tan\left(\frac{\vec{k}_x \Omega_h}{2}\right)}{\vec{k}_x}, & \text{if } \vec{k}_x > 0 \\ \frac{\Omega_h}{2}, & \text{if } \vec{k}_x = 0 \\ \frac{\sin\left(\frac{\vec{k}_x \Omega_h}{2}\right)}{\vec{k}_x}, & \text{if } \vec{k}_x < 0 \end{cases} \quad (3)$$

where $\Omega_h \in (0, \tau]$ denotes horizontal angle of view. Similarly vertical Ω_v can be obtained using \vec{k}_y parameter instead. Result value $1/f \in \mathbb{R}_{>0}$ is the reciprocal focal-length.

Remark. Focal-length f value must be same for $\vec{\theta}_x$ and $\vec{\theta}_y$. Therefore only one reference angle Ω can be chosen, either horizontal or vertical.



(a) Graph illustrating correlation between angle φ and anamorphic interpolation vector $\vec{\varphi} \in [0, 1]^2$. Here angle φ is illustrated as 2-times scaled, arc of 180° .



(b) Graph mapping angle φ , to anamorphic interpolation weights $\vec{\varphi}_x$ and $\vec{\varphi}_y$. Illustrates circular distribution of $\vec{\varphi}$, in a periodic function.

Figure 1. Illustrating correlation between anamorphic interpolation weights $\vec{\varphi}$ and spherical angle φ .

Inverse function to Equation (3), for angle-of-view Ω from focal-length f , is obtained as follows

$$\Omega_v(f) = \begin{cases} \frac{2 \arctan(\frac{\vec{k}_y}{f})}{\vec{k}_y}, & \text{if } \vec{k}_y > 0 \\ \frac{2}{f}, & \text{if } \vec{k}_y = 0 \\ \frac{2 \arcsin(\frac{\vec{k}_y}{f})}{\vec{k}_y}, & \text{if } \vec{k}_y < 0 \end{cases} \quad (4)$$

This can be used to obtain actual vertical angle-of-view from horizontally established focal length. Similarly horizontal angle Ω_h can be obtained using \vec{k}_x parameter.

2.2 Vignetting mask

Vignetting is an important visual symbol indicating projection stretching of the visual sphere. Incorporating vignetting effect increases space perception.

Here anamorphic vignetting mask Λ' is obtained similarly to anamorphic angle θ' . Two separate vignetting masks, $\vec{\Lambda}_x$ and $\vec{\Lambda}_y$ are generated for each power axis and combined to a single anamorphic vignette Λ' by interpolation through $\vec{\varphi}$ component-weights.

$$\begin{bmatrix} \vec{\Lambda}_x \\ \vec{\Lambda}_y \end{bmatrix} = \begin{bmatrix} \left| \cos \left(\max \{ |\vec{k}_x|, \frac{1}{2} \} \vec{\theta}_x \right) \right|^{\frac{k_x+3}{2}} \\ \left| \cos \left(\max \{ |\vec{k}_y|, \frac{1}{2} \} \vec{\theta}_y \right) \right|^{\frac{k_y+3}{2}} \end{bmatrix} \quad (5a)$$

$$\Lambda' = \begin{bmatrix} \vec{\Lambda}_x \\ \vec{\Lambda}_y \end{bmatrix} \cdot \begin{bmatrix} \vec{\varphi}_x \\ \vec{\varphi}_y \end{bmatrix}, \quad \square \quad (5b)$$

where $\Lambda' \in [0, 1]$ is the anamorphic vignetting mask value, interpolated using circular-function vector $\vec{\varphi}$.

Vignette mask of each axis is obtained using two laws of illumination falloff. Inverse-square law (for $k = 1$) and cosine law of illumination (for $k = -1$). Vignette value for *cosine law* of illumination is simply expressed as $\cos \theta'$. *Inverse-square law* value can be expressed as $\cos^2 \theta'$. Therefore value for projections other

than $k \in \{-1, 1\}$ must have vignetting value in-between $\cos^1 \theta' \leftrightarrow \cos^2 \theta'$. This has been empirically evaluated to a power value linearly-mapped from $k \in [-1, 1] \mapsto [1, 2]$.

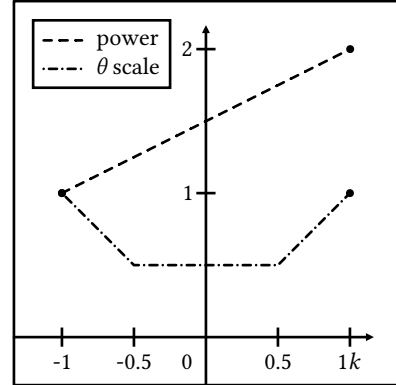


Figure 2. Graph illustrating interpolation parameters for anamorphic vignetting (vertical axis value), driven by $k \in [-1, 1]$ parameter (horizontal axis). *Power* graph ($\frac{k+3}{2}$) interpolates between *cosine law of illumination* and *inverse-square law* vignetting. *θ-scale* graph scales vignetting boundary.

3 Converting ray-map to ST-map

Ray/perspective-map can be easily converted to the *ST*-map, given that maximum view angle does not exceed or isn't equal 180° .

$$\begin{bmatrix} \vec{a}_x & \vec{a}_y \end{bmatrix} = \begin{cases} \begin{bmatrix} 1 & \frac{w}{h} \end{bmatrix}, & \text{if } \Omega_h \\ \begin{bmatrix} \frac{h}{w} & 1 \end{bmatrix}, & \text{if } \Omega_v \end{cases} \quad (6a)$$

$$\begin{bmatrix} \vec{f}_s \\ \vec{f}_t \end{bmatrix} = \frac{\cot \frac{\Omega}{2}}{2\hat{G}_z} \begin{bmatrix} \hat{G}_x \\ \hat{G}_y \end{bmatrix} \begin{bmatrix} \vec{a}_x \\ \vec{a}_y \end{bmatrix} + \frac{1}{2}, \quad \square \quad (6b)$$

Value of k	Azimuthal projection type
$k_i = 1$	Rectilinear (aka Gnomonic)
$k_i = 1/2$	Stereographic
$k_i = 0$	Equidistant
$k_i = -1/2$	Equisolid
$k_i = -1$	Orthographic (azimuthal)

Source: PTGui 11 fisheye factor [Krause 2019].

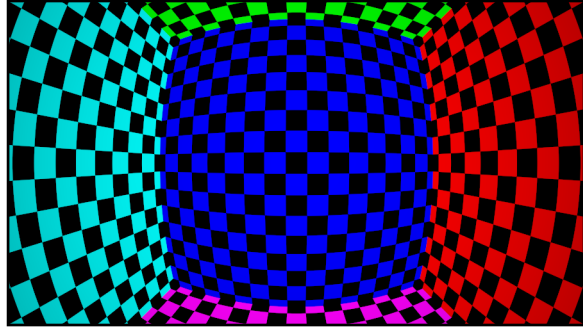
(a) Azimuthal projection type and corresponding k value.

Azimuthal projection type	Perception of space
Rectilinear	straightness
Stereographic	shape, angle
Equidistant	speed, aim
Equisolid	distance, size
Orthographic	—

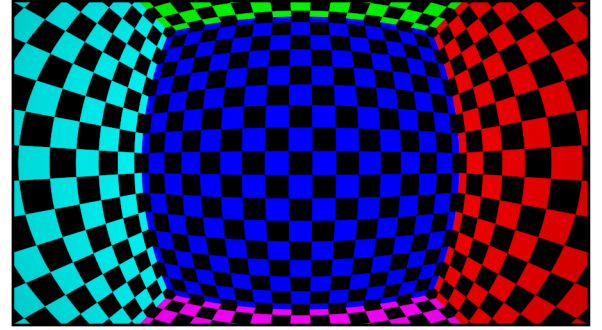
Source: Empirical study using various competitive video games.

(b) Correct perception of space attributes and corresponding azimuthal projection type.

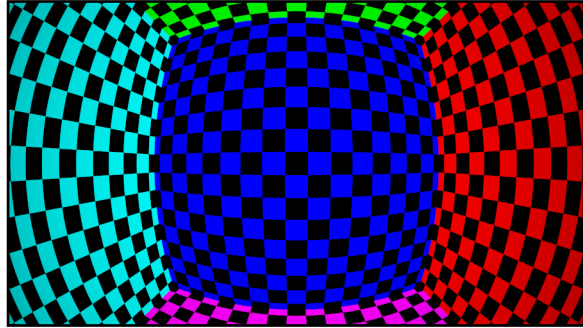
Table 1. Tables presenting perspective parameters, corresponding projection type and associated perception attitude.



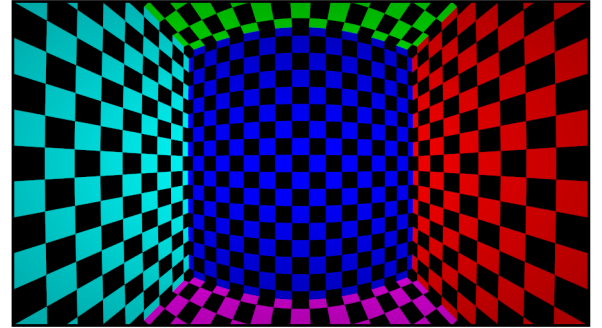
(a) $\vec{k} = [0 \quad 1/2]$ first-person.



(b) $\vec{k} = [1/2 \quad -1/2]$ racing.



(c) $\vec{k} = [-1/2 \quad 0]$ flying.



(d) $\vec{k} = [1/2 \quad 1]$ panini.

Figure 3. Example of various wide-angle ($\Omega_v = 100^\circ$) anamorphic azimuthal projections with vignetting in 16:9 aspect-ratio. Checkerboard depicts cube centered at the view-position, with each face colored according to axis direction. Here primary colors represent positive axis and complementary colors its opposite equivalent (same as in color-wheel), $\{Cy, Mg, Yl\} \leftrightarrow -\{X, Y, Z\} \mapsto \{R, G, B\}$.

where $\vec{a} \in \mathbb{R}^2$ is the square-mapping vector for horizontal and vertical angle of view. Values w and h represent picture width and height respectively. $\Omega < \pi$ is the angle of view. $\vec{f} \in [0, 1]^2$ represents the final ST -map vector and $\hat{G} \in [0, 1]^3$ is the input primary-ray map vector.

4 Anamorphic lens distortion

Presented perspective model can be used to simulate real-world anamorphic lens. It can incorporate effects such as *disproportionate lens breathing*, which are unique to anamorphic photography [Sasaki 2017b] thanks to being focal-length based. Some additional lens-correction may be added to the primary-ray map, to compensate for lens imperfections.

Below presented is an algorithm for anamorphic distortion of view coordinates, which can be used as an input for

Picture content type	Anamorphic \vec{k} values
Racing simulation	$\vec{k} = \begin{bmatrix} 1/2 & -1/2 \end{bmatrix}$
Flying simulation	$\vec{k} = \begin{bmatrix} -1/2 & 0 \end{bmatrix}$
Stereopsis (cyclopean)	$\vec{k} = \begin{bmatrix} 0 & -1/2 \end{bmatrix}$
First-person shooting	$\vec{k} = \begin{bmatrix} 0 & 1/2 \end{bmatrix}$
Pan motion	$\vec{k}_x \neq \vec{k}_y$
Roll motion	$\vec{k}_y = \vec{k}_x$
Tilt motion ^a	$\vec{k}_y \rightarrow \vec{k}_x$

Source: Determined empirically using various competitive video games, in accordance to data in Table 1b.

^aMapping of vertical distortion by a tilt motion introduced first in a Minecraft mod [Williams 2017].

Table 2. Recommended values of \vec{k} for various content type.

primary-ray map algorithm. It is based on *Brown-Conrady* lens-distortion model [Wang et al. 2008] in a division-variant [Fitzgibbon 2001]. It is executed upon view-coordinates \vec{v} , forming alternative \vec{v}' .

$$\begin{bmatrix} \vec{f}_x \\ \vec{f}_y \end{bmatrix} = \underbrace{\begin{bmatrix} \vec{v}_x - \vec{c}_1 \\ \vec{v}_y - \vec{c}_2 \end{bmatrix}}_{\text{cardinal offset } a} \quad (7a)$$

$$\begin{bmatrix} \vec{\varphi}_x \\ \vec{\varphi}_y \end{bmatrix} = \begin{bmatrix} \frac{\vec{f}_x^2}{\vec{f}_x^2 + \vec{f}_y^2} & \frac{\vec{f}_y^2}{\vec{f}_x^2 + \vec{f}_y^2} \end{bmatrix}^T \quad (7b)$$

$$r^2 = \vec{f}_x^2 + \vec{f}_y^2 \quad (7c)$$

$$\begin{bmatrix} \vec{v}'_x \\ \vec{v}'_y \end{bmatrix} = \underbrace{\begin{bmatrix} \vec{f}_x \\ \vec{f}_y \end{bmatrix} \left(\begin{bmatrix} 1 + \vec{k}_{x1}r^2 + \vec{k}_{x2}r^4 \dots \\ 1 + \vec{k}_{y1}r^2 + \vec{k}_{y2}r^4 \dots \end{bmatrix} \cdot \begin{bmatrix} \vec{\varphi}_x \\ \vec{\varphi}_y \end{bmatrix} \right)^{-1}}_{\text{radial anamorphic}} \quad \square \quad (7d)$$

$$+ \underbrace{\begin{bmatrix} \vec{f}_x \\ \vec{f}_y \end{bmatrix} \left(\begin{bmatrix} \vec{f}_x \\ \vec{f}_y \end{bmatrix} \cdot \begin{bmatrix} \vec{p}_1 \\ \vec{p}_2 \end{bmatrix} \right)}_{\text{decentering}} + \underbrace{r^2 \begin{bmatrix} \vec{q}_1 \\ \vec{q}_2 \end{bmatrix}}_{\text{thin prism}} + \underbrace{\begin{bmatrix} \vec{c}_1 \\ \vec{c}_2 \end{bmatrix}}_{\text{cardinal } b} \quad \square$$

$$\begin{bmatrix} \vec{v}'_x \\ \vec{v}'_y \end{bmatrix} \mapsto \begin{bmatrix} \hat{G}_x \\ \hat{G}_y \\ \hat{G}_z \end{bmatrix}, \quad \square \quad (7e)$$

where \vec{c}_1, \vec{c}_2 are the cardinal-offset parameters, \vec{q}_1, \vec{q}_2 are the thin-prism distortion parameters and \vec{p}_1, \vec{p}_2 are the decentering parameters. Set of \vec{k} parameters define radial distortion for each anamorphic power axis. \vec{v} is the input view-coordinate and \vec{v}' is the view coordinate with applied lens-transformation. $\vec{\varphi} \in [0, 1]^2$ is the anamorphic interpolation weight, defined in Section 2 on page 2.

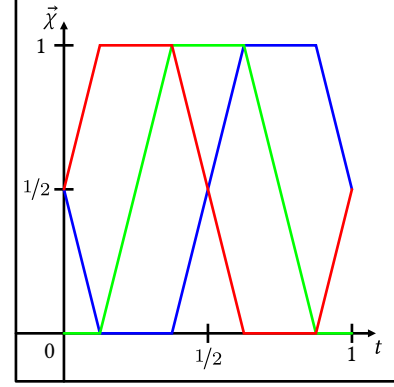


Figure 4. Graph mapping of $t \in [0, 1]$ to spectral color $\vec{\chi} \in [0, 1]^3$, for simulation of chromatic aberration. This is an output of periodic function found in Equation (8). Distribution of values ensures proper color order and sum of samples equal to neutral-white.

5 Anamorphic chromatic aberration

Chromatic aberration effect can be achieved with multi-sample blur, where each sampled layer is colored by the corresponding spectral-value [Gilcher 2015]. Presented periodic function for spectral color $\vec{\chi}$ produces samples that always add-up to 1 (neutral white), when number is even. It also presents correct order of spectrum colors.

$$\begin{bmatrix} \vec{\chi}_r \\ \vec{\chi}_g \\ \vec{\chi}_b \end{bmatrix} = \underset{0}{\overset{1}{\text{clamp}}} \left(\frac{3}{2} - \left| 4 \bmod \left(t + \begin{bmatrix} 1/4 \\ 0 \\ 3/4 \end{bmatrix}, 1 \right) - 2 \right| \right), \quad (8)$$

where $\vec{\chi} \in [0, 1]^3$ is the spectral-color value for position $t \in [0, 1]$. See Figure 4 for more information.

Performing spectral blur on an image involves multi-sample sum of spectrum-colored layers. Here t (replaced by sample progress) never reaches 1, this preserves picture white-balance. Number of samples n must be an even number, no less than 2, for a correct result.

$$\begin{bmatrix} \vec{f}'_r \\ \vec{f}'_g \\ \vec{f}'_b \end{bmatrix} = \frac{2}{n} \sum_{i=0}^{n-1} \begin{bmatrix} \vec{f}_r \\ \vec{f}_g \\ \vec{f}_b \end{bmatrix} \underbrace{\underset{0}{\overset{1}{\text{clamp}}} \left(\frac{3}{2} - \left| 4 \bmod \left(\frac{i}{n} + \begin{bmatrix} 1/4 \\ 0 \\ 3/4 \end{bmatrix}, 1 \right) - 2 \right| \right)}_{\vec{\chi} \text{ periodic function}}, \quad (9)$$

where $n \in 2\mathbb{N}_1$ is the even number of samples for the chromatic aberration color-split. $\vec{f} \in [0, 1]^3$ is the current-sample position color value. $\vec{f}' \in [0, 1]^3$ is the final spectral-blurred color value.

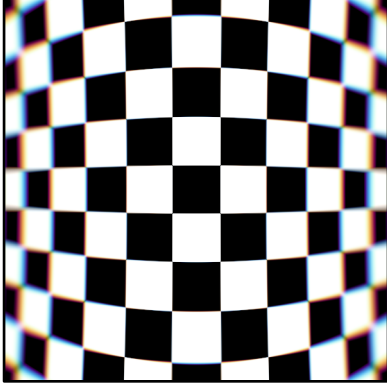


Figure 5. Example of anamorphic lens distortion with chromatic aberration, $\vec{k}_{x1} = -0.25$, $\vec{k}_{y1} = 0.04$, $d = 0.5$, 64-samples.

Equation for spectral color $\vec{\chi}$ can be rewritten to more computationally optimized form.

$$\begin{bmatrix} \vec{\chi}_r \\ \vec{\chi}_g \\ \vec{\chi}_b \end{bmatrix} = \begin{bmatrix} \text{clamp}_0^1(3/2 - |4t - 1|) \\ \text{clamp}_0^1(3/2 - |4t - 2|) \\ -\text{clamp}_0^1(3/2 - |4t - 1|) \end{bmatrix} + \begin{bmatrix} \text{clamp}_0^1(4t - 7/2) \\ 0 \\ 1 - \text{clamp}_0^1(4t - 7/2) \end{bmatrix}, \quad (10)$$

where $\vec{\chi} \in [0, 1]^3$ is the spectral color at position $t \in [0, 1]$. See Figure 4 on the previous page for visualization.

5.1 Chromatic aberration through lens distortion

Chromatic aberration can be integrated into lens distortion, by spectral blurring through distortion-transformation vector $\vec{v}_\Delta = \vec{v}' - \vec{v}$. Below presented is equation for spectral-blur displacement vector, calculated per spectral-blur sample.

$$\vec{v}_\Delta(t) = \left(1 + (2t - 1)\frac{d}{2}\right)\vec{v}_\Delta, \quad (11)$$

where $\vec{v}_\Delta(t) \in \mathbb{R}^2$ is the spectral blur sample-offset vector at position $t \in [0, 1]$. Value $d \in \mathbb{R}$ denotes lens dispersion-scale.

6 Final thoughts

In this article mathematical model for designing anamorphic perspective geometry has been presented. Parametrization of this model enables adaptive picture geometry, which can be dynamically adjusted to the visible content, in an artistically convincing manner. Along with anamorphic perspective, vignetting and lens-distortion with chromatic-aberration has been provided, for a holistic digital-lens experience.

References

Leon B. Alberti. 1435. *On Painting* (1970 ed.). New Haven: Yale University Press. <http://www.noteaccess.com/Texts/Alberti/index.htm>

Giulio C. Argan and Nesca A. Robb. 1946. The Architecture of Brunelleschi and the Origins of Perspective Theory in the Fifteenth Century. *Journal of the Warburg and Courtauld Institutes* 9 (1946), 96. <https://doi.org/10.2307/750311>

Joseph Baldwin, Alistair Burleigh, and Robert Pepperell. 2014. Comparing Artistic and Geometrical Perspective Depictions of Space in the Visual Field. *i-Perception* 5, 6 (jan 2014), 536–547. <https://doi.org/10.1068/i0668>

Felix Bettonvil. 2005. Fisheye lenses. *WGN, Journal of the International Meteor Organization* 33, 1 (2005), 11–12. https://ui.adsabs.harvard.edu/link_gateway/2005JIMO...33....9B/ADS_PDF

José Correia and Luís Romão. 2007. Extended perspective system. In *Proceedings of the 25th eCAADe International Conference*. 185–192.

Leonardo Da Vinci. 1632. *A treatise on painting* (2014 ed.). Project Gutenberg, Chapter Linear Perspective, 49–59. <http://gutenberg.org/ebooks/46915>

Robert A. Dixon. 1987. *Mathographics*. Basil Blackell Limited, Chapter Perspective Drawings, 82–83.

Andrew W. Fitzgibbon. 2001. Simultaneous linear estimation of multiple view geometry and lens distortion. In *Proceedings of the 2001 IEEE Computer Society Conference on Computer Vision and Pattern Recognition. CVPR 2001*, Vol. 1. IEEE Comput. Soc, Kauai, HI, USA. <https://doi.org/10.1109/cvpr.2001.990465>

Margaret M. Fleck. 1994. *Perspective Projection: the Wrong Imaging Model*. techreport 95-01. Computer Science, University of Iowa. <https://mfleck.cs.illinois.edu/my-papers/stereographic-TR.pdf>

Daniel M. German, Pablo D'Angelo, Michael Gross, and Bruno Postle. 2007. New Methods to Project Panoramas for Practical and Aesthetic Purposes. In *Computational Aesthetics in Graphics, Visualization, and Imaging*. The Eurographics Association. <https://doi.org/10.2312/COMPAESTH/COMPAESTH07/015-022>

Carolyn Giardina. 2016. How 'The Hateful Eight' Cinematographer Revived Lenses From the 1960s. *The Hollywood Reporter* (Jan. 2016). <https://hollywoodreporter.com/news/how-hateful-eight-cinematographer-revived-852586> Online.

Pascal Gilcher. 2015. YACA (Yet Another Chromatic Aberration). ReShade forum. <https://reshade.me/forum/shader-presentation/1133-yaca-yet-another-chromatic-aberration#8861> Forum post.

Rudolf Kingslake. 1989. *A History of the Photographic Lens*. Academic Press, Chapter IV, 59–62.

Erik Krause. 2019. *Fisheye Projection*. PanoTools wiki. https://wiki.panotools.org/index.php?title=Fisheye_Projection&oldid=16077 Online.

James M. McArdle. 2013. From the corner of your eye?... Personal blog. <https://drjamesmcardle.com/2013/04/07/from-the-corner-of-your-eye/> Online.

Luis Peñaranda, Luiz Velho, and Leonardo Sacht. 2015. Real-time correction of panoramic images using hyperbolic Möbius transformations. *Journal of Real-Time Image Processing* 15, 4 (may 2015), 725–738. <https://doi.org/10.1007/s11554-015-0502-x>

Dan Sasaki. 2017a. The Aesthetics of Anamorphic in Film and Digital. Panavision Inc. <https://vimeo.com/167052303> Video.

Dan Sasaki. 2017b. The Five Pillars of Anamorphic - Disproportionate Breathing. Panavision Inc. <https://vimeo.com/167045643> Video.

Thomas K. Sharpless, Bruno Postle, and Daniel M. German. 2010. Panini: A New Projection for Rendering Wide Angle Perspective Images. *Computational Aesthetics in Graphics Visualization, and Imaging* (2010). <https://doi.org/10.2312/COMPAESTH/COMPAESTH10/009-016>

Jianhua Wang, Fanhuai Shi, Jing Zhang, and Yuncai Liu. 2008. A new calibration model of camera lens distortion. *Pattern Recognition* 41, 2 (feb 2008), 607–615. <https://doi.org/10.1016/j.patcog.2007.06.012>

Eric J. W. Whittaker. 1984. *The Stereographic Projection* (2001 ed.). University College Cardiff Press. <http://oldwww.uicr.org/uicr-top/comm/cteach/pamphlets/11/11.pdf>

Wikipedia, contributors. 2019. Robert Barker (painter). *Wikipedia, The Free Encyclopedia* (2019). [http://en.wikipedia.org/w/index.php?title=Robert_Barker_\(painter\)&oldid=907715733#Biography](http://en.wikipedia.org/w/index.php?title=Robert_Barker_(painter)&oldid=907715733#Biography)

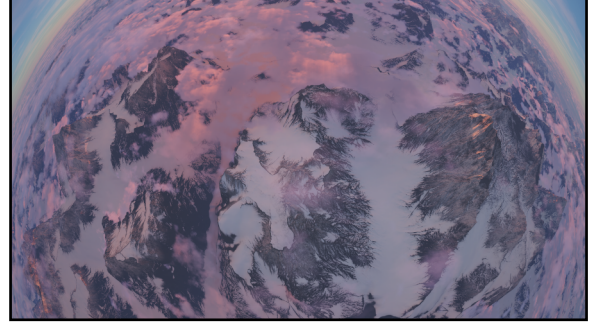
Shaun E. Williams. 2015. Blinky. GitHub, Inc. <https://github.com/shaunlebron/blinky> Modification, Quake.

Shaun E. Williams. 2017. Flex FOV. GitHub, Inc. <https://github.com/shaunlebron/flex-fov> Modification, Minecraft.



Panorama source: Grzegorz Wronkowski, CC-BY.

(a) Racing, $\vec{k} = [1/2 \quad -1/2]$, $f = 0.58$, $\Omega_h \approx 163^\circ$



Panorama source: Grzegorz Wronkowski, CC-BY.

(b) Flying, $\vec{k} = [-1/2 \quad 0]$, $f = 0.74$, $\Omega_h \approx 170^\circ$



Panorama source: captured from OBDUCTION through Nvidia Ansel.

(c) First-person, $\vec{k} = [0 \quad 1/2]$, $f = 0.82$, $\Omega_h \approx 140^\circ$



Panorama source: captured from FOR HONOR through Nvidia Ansel.

(d) Stereopsis, $\vec{k} = [0 \quad -1/2]$, $f = 0.63$, $\Omega_h \approx 182^\circ$

Figure 6. Examples of super-wide angle views in anamorphic projection, mapped from equirectangular panoramas.